Integrated wavelength monitoring in a photonic-crystal tunable laser diode

Holger Friedrich Hofmann, Martin Kamp, Alfred Forchel, Dominic F.G. Gallagher, Henri Benisty

Integrated wavelength monitoring in a photonic-crystal tunable laser diode

H. Hofmann [a], M. Kamp [a], A. Forchel [a], D. Gallagher [b], H. Benisty [c,*]

[a] *Department of Physics, Microstructure Laboratory, Julius-Maximilians-Universität Würzburg, 97074 Würzburg, Germany*
[b] *Photon Design, OX4 1TW Oxford, UK*
[c] *Laboratoire Charles Fabry de l'Institut d'Optique, CNRS, Univ Paris-Sud, Campus Polytechnique, RD 128, F-91127 Palaiseau, France*

A photonic-crystal tunable 1.55 μm laser diode is fitted with a wavelength monitor on its rear side. The 250-μm long laser based on a coupled-cavity design has approximately 15 nm tunability. The wavelength monitor collects and differentially feeds two-photodetecting areas, thanks to a mode conversion to a higher-order mode (a mini-stopband), followed by tunneling through a thin clad. The layout is numerically optimized to minimize unwanted reflections. Electrical cross-talk was prevented through guard rings and trenches. The correlation between wavelength and the monitor photocurrent ratio demonstrates a 10–20 GHz stabilization capability, or a 15 nm monitoring range.

Keywords: Photonic crystal; Tuneable laser; Integration; Telecommunications; Spectrometer; Mode coupling; InP

1. Introduction

Tunable laser diodes for telecom applications have been continuously improved in the last two decades [1]. The advent of photonic-crystal-(PhC) based devices has enabled a revival of early attempts to achieve tunability via coupled-cavity design. Mahnkopf et al. [2–4] have demonstrated tunability together with reasonable output power from such two-section PhC lasers. In all these schemes, there is no simple correlation between the two currents and the selected wavelength. As a result, a pre-test and a look-up table are required before use. It is clear that with this complexity, unavoidable in this scheme even with clever design, wavelength stability is more intrinsically at stake than in standard phase-shifted or complex-coupled DFB lasers [5,1]. In order to deal with the issue of wavelength stability, an external, hybrid wavelength locker is combined with a tunable laser, and in case of high wavelength stability, also with a fixed wavelength laser. These wavelength lockers are usually Fabry–Perot (FP) etalons with a free spectral range that is compatible with an ITU channel spacing (e.g. 100 GHz) [6]. The etalon transmission is monitored, i.e. the beam is split before the FP, and the intensity through the FP is compared to that in direct pass. If the wavelength of the tunable laser can be coarsely tuned with an accuracy of less than half of the free spectral range of the locker, then the locker can be used for a fine adjustment of the emission wavelength on the target value. An integrated monolithic solution is of course preferable insofar as packaging costs are concerned [7–9]. It is also more elegant, except for the delicate issue of temperature

* Corresponding author.
E-mail address: henri.benisty@polytechnique.fr (H. Benisty).

stabilization, the thermal index $n_T = \partial n/\partial T$ of semiconductors being much larger than that of glass or special a thermal materials [6] for instance. Semiconductors such as InP are known to produce a $\sim$0.1 nm/K shift of spectral features at 1550 nm, through the combination of index change and physical path expansion.

It is therefore desirable to investigate practical implementations for spectral monitoring of tunable laser, to further ensure their stabilization inside complex systems. Here we propose an all PhC-based wavelength monitoring scheme. PhC lasers with liquid crystal tuning were demonstrated earlier [10], but we use a simpler two-cavity scheme here. We report on three aspects of photonic technology and design that were found necessary when investigating a compact integrated PhC monitor for the novel PhC-based coupled-cavity lasers [11,12]. We firstly report on the design choice and the operation of our particular selective ''mini-stopband'' (MSB) selective monitoring device. We also report, secondly, on the photonic and optoelectronic design improvements. We eventually report on the tests of a device implementing these designs. The wavelength/monitor signal correlation was found monotonous and unambiguous enough to result in principle in 20 GHz stabilization. On a broader range, equivocal situations (with different wavelengths providing the same current ratio) arose, but still, a fair discrimination over more than 15 nm appeared. Note that as the large majority of tunable laser diodes, the discrimination is intrinsically delicate around mode jumps, when the side mode suppression ratio (SMSR) collapses to modest values. But we could characterize the high SMSR situations in quite some detail.

2. Lasers and photodetection

Coupled-cavity lasers used here exploit the presence of two frequency combs with a modest difference in their individual free spectral ranges (FSR) in a double segment PhC cavity resonator (Fig. 1a). Each cavity segment is a closed ''W9'' waveguide, meaning that 9 PhC rows are omitted along ΓK direction to define the PhC guide across the InP-based laser diode heterostructure. A standard laser structure (shown in Fig. 1b) with six compressively strained quantum wells was used. The quantum wells provide gain for TE polarized light around 1550 nm, matched to the bandgap of the PhC for a typical air-filling factor of $f = 35\%$. Each comb stems from a cavity, and since the two cavities have lengths of 110 and 140 μm, their FSRs are in the same 11:14 ratio.

When current is injected separately in each section, the respective frequency combs drift by a differential amount dictated by the temperature rise of each segment. Since the lasers are fabricated from all-active material, the carrier densities in the quantum wells vary only slightly with injection current once both segments have reached threshold. As a result of the coupling between the two cavities by a two-rows-thick PhC mirror, laser oscillation takes place at the wavelength best favored by the coincidence of comb teeth (the so-called Vernier effect), and may therefore be tuned across the material gain curve. More data on the technology details can be found in [4]. Tuning over 15 nm is achievable on the particular devices used here. The output mirror (the single column of holes in Fig. 1a) is separated from the anti-reflection coated cleaved facet, so that the two cavities have both deterministic lengths and end reflectivities.

Using the same laser heterojunction in reverse bias transforms the system into a guided wave photodetector, with a fraction of A/W responsivity. The aim of the present work is to define a sub-device arrangement at the rear of the coupled-cavity laser so as to monitor the emitted wavelength on the chip, for instance by looking

(a)

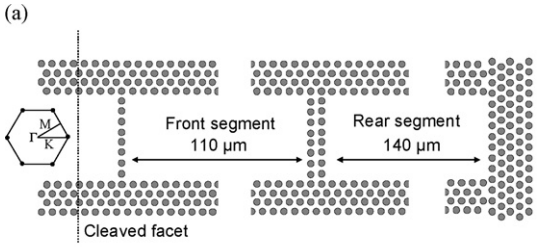

(b)

Layer	Material	Thickness
Contact layer	InGaAs, Q 1.65	250 nm
Upper cladding	p-InP	1200 nm
SCH	InGaAsP Q 1.17	60 nm
Active layer 6 QWs and 5 barriers	InGaAsP Q 1.55 QW InGaAsP Q 1.17 barrier	8 nm 10 nm
SCH	InGaAsP Q1.17	60 nm
Lower cladding or buffer	n-InP	1000 nm

Fig. 1. (a) Principle of the photonic-crystal coupled-cavity tunable laser. The PhC used for the mirrors is rotated by 90° with respect to that of the waveguide in order to achieve high reflectivities. Light impinging on a PhC mirror along the ΓK direction would be mainly diffracted. (b) Layer structure of the 1550 nm laser. The thickness of the upper cladding layer is smaller than usual in order to relax the demands on the aspect ratio of the etched holes which have to penetrate the complete vertical structure.

at a pair of photocurrents that depend in a controllable fashion on the emitted optical frequency.

3. Design issue

Since external monitoring often makes use of FP slabs, it is natural to think of implementing a wavelength monitor with a PhC-based FP cavity. However, this entails several difficulties. Firstly, the FP resonators only work in a narrow range of FSR. Secondly, a splitter has to be inserted before the FP, because the comparison has to be made between FP signal inserted in one of the splitter's arm, and a reference on the other arm.

Recently, a specific feature of PhC multimode waveguides was proposed to accomplish wavelength demultiplexing via the mini-stopband extraction mechanism [13]. When light is launched into the fundamental mode of a PhC waveguide, it sees the PhC corrugation on both sides. However, a strong diffracted signal is not generated unless a radiation hits a higher-order mode (a transverse resonance condition), a condition which occurs only in a narrow frequency/momentum window called the MSB. This was explained in [14] and further exploited for demultiplexing action in several papers [15–18]). One of the PhC waveguide lateral walls has to be thinned to tap out the higher-order mode generated by the modal conversion, leaving the fundamental mode and the other wavelengths virtually unaffected.

The MSB of a W3 PhC waveguide offers good operation conditions—the interaction is strong enough at resonance for the modal conversion to occur in only a couple of PhC periods inside the waveguide, and the guide is still wide enough to permit coupling from the broader laser waveguide without excessive difficulties.

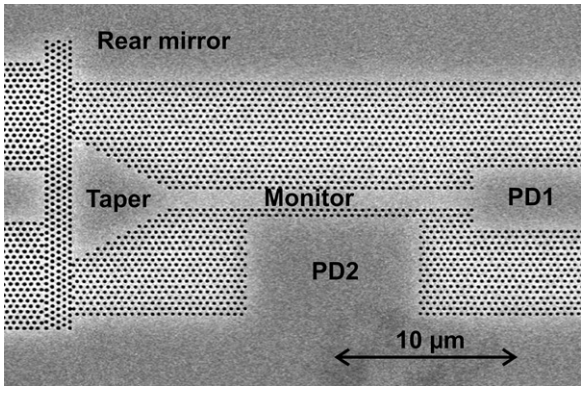

Fig. 2. First generation monitor layout. Light from the back of the laser is funneled through the taper to the monitor section, where it is selectively dropped to PD2 at the mini-stopband frequency.

A first generation device layout can be seen in Fig. 2. At the back of the W9 laser guide, there are five PhC rows acting as a high reflectivity mirror with only ∼5% transmission. The transmitted wave is funneled by means of a short taper [19] into an 8-μm long W3 waveguide acting as the wavelength monitor. At the end of this W3 waveguide is located the first photodiode PD1. One of the sides of the W3 cladding is thinned to two rows, causing leakage into the second photodiode PD2. The micrograph in Fig. 2 is taken before the electrical contacts were implemented.

In a series of experiment based on this first design, two major shortcomings were encountered. Firstly, the laser tunability was compromised. Secondly, there was a large electrical leakage among the photodiodes, and also between the photodiode and the laser rear section. The compromised tunability was diagnosed to result from spectrally selective feedback, notably from partial reflection of the fundamental mode at the entrance of the W3 waveguide at the wavelength of its MSB. For a mode already inside the guide, it is converted to a higher-order mode as indicated above, but for light from outside, simulations indicate that a sizable reflection occurs, typically 20–40%, depending on the interplay with the geometry outside the guide (here the taper). The electrical leakage is a consequence of the absence of a *bona fide* insulation between the p-doped conductive regions, allowing voltage swings at one point to ''ohmically'' influence diodes in the far vicinity.

The electrical leakage was suppressed by trenches which are etched through the entire p–n junction, leading to a complete electrical isolation of the photodiode PD2 lateral to the W3 waveguide. Although this introduces some non-radiative recombination at the open sidewalls, the photocurrent is not significantly reduced thanks to the small surface recombination velocity of the InGaAsP/InP material system. Another precaution was to insert guard rings around the photodiode area, to force a zero equipotential around them. We tried metallic guard rings alone, situated on top of the device, and hence with only minute photonic effects given the way the waveguide modes are buried. However this did not suppress well enough the electrical cross-talk between the two photodiodes. Hence we had to add trenches around PD2 to attain sufficient insulation.

In order to address the optical design issues, we carried out FDTD analysis of our device which we shall detail now. The issue at hand is twofold. (i) What would the impact of insulating trenches be on the demultiplexer selectivity? and (ii) how can the back reflection

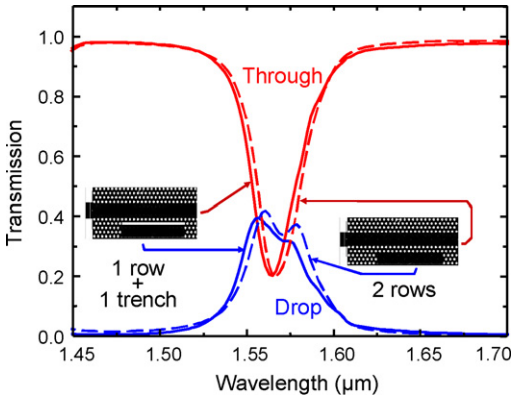

Fig. 3. Transmission spectra showing the small photonic influence of the replacement of the outer PhC row by a trench in the thinned W3 cladding.

of the fundamental mode at the entrance of W3 be reduced? we first studied a system where the second row of holes in the thin cladding of W3 is replaced by a trench. We used crystalwave [20] to model the device. This software is based on an FDTD algorithm. In Fig. 3, we show two designs for an 8 μm photodiode, a W3 waveguide with a cladding thinned down to two rows in the basic case, the outermost row being replaced by the insulating trench in the modified case.

The simulation results indicate that the drop efficiency is almost unchanged by the replacement, only minor spectral shape changes can be detected. This trend could be expected because the interaction between the two modes is mainly defined by the corrugation seen by the fundamental mode at the inner PhC rows, and has very limited contribution from the second row (see e.g. Ref. [21] for the use of second row for very fine tuning).

A further step is to reduce reflection at the entrance. For this purpose, a first idea is to ascribe the reflection in the fundamental mode to the forbidden transmission of energy in the MSB gap, in either direction. Then, tapping the electromagnetic energy of the waveguide to the photodiode may imbalance the underlying electromagnetic response, and ease the incoming energy penetration, by frustrating the elementary hole reflections that, in essence, collectively forbid energy transport in the W3 waveguide at the MSB condition. We therefore checked whether approaching the PD2 section directly at the entrance would diminish reflection. The reason for the initial design was a naive belief that the modes need to "shape up" in the W3 waveguide for proper action. However, given the slightly backward propagation of the useful higher-order mode, this is essentially not true. The short version of Fig. 4b, diverting the desired mode right at the entrance was found to maintain the selectivity of the drop signal, while considerably assisting the desired reflection suppression (Fig. 4d, violet dashed curve), by a factor of four roughly.

Still, damping the local resonator operation does not act so specifically toward the input reflection. To reduce the reflection further, we created a second reflection by introducing a dislocation at the pth period inside the W3 waveguide for $p = 1$–5. The dislocation is a simple $a/2$ shift (Fig. 4c) and its reflection is designed to destructively interfere with the reflection at the beginning of the device so reducing the total reflection. We found that $p = 3$ ensured the best result, as can be seen in Fig. 4d: reflection goes down to a few percent with this choice. This value $p = 3$ is, not so surprisingly, on the order of the higher-order mode coupling distance

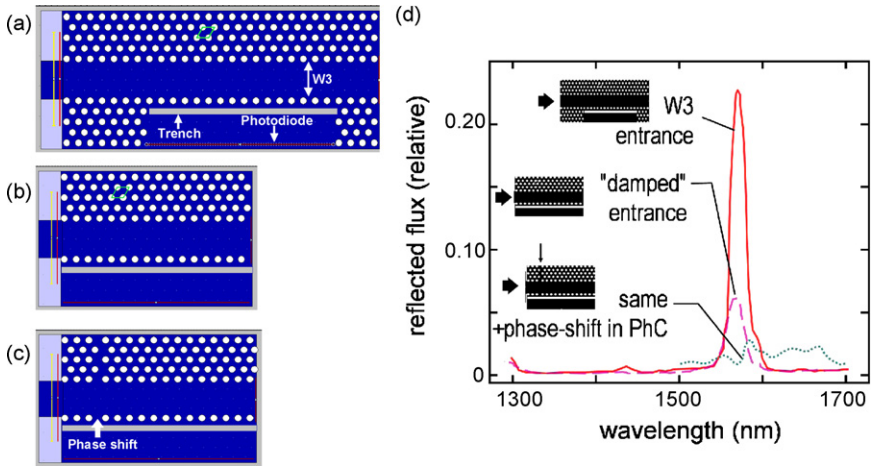

Fig. 4. (a) Design with W3 entrance (photodiode starts at the 7th period); (b) photodiode directly at entrance, no dislocation; (c) photodiode directly at entrance, dislocation at third period; (d) relative reflected fluxes for the three designs.

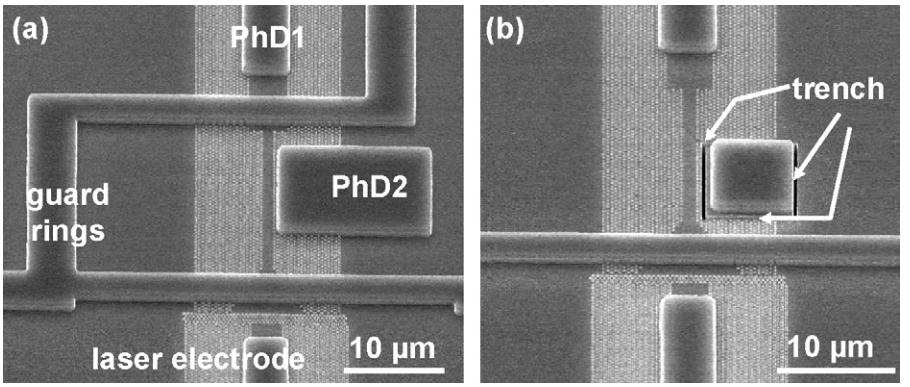

Fig. 5. Micrographs of almost finished devices; (a) initial design (no trench, W3 guide before PD2); (b) one of the improved designs (trench all around PD2, suppression of the W3 section before it); no dislocation in this particular sample.

($\sim v_g/c\kappa$, in the classical terminology of coupled mode theory practitioners) [22].

4. Fabrication and results

Fig. 5a and b shows micrographs of almost finished devices (planarization and top contact still missing), with either the basic design (no trench, no precaution against reflection), or the improved design version without the dislocation (as in Fig. 4b).

Fabrication proceeded essentially as described for the coupled-cavity photonic-crystal laser diodes earlier [4]. The trenches are defined together with the PhCs, so no extra level of lithography is required. The etch depth of the trenches is similar or even larger than that of the holes (≈3.5 µm) which ensures a complete isolation of the lateral photodiode. The guard rings are defined together with the contacts to the laser segments and the photodiodes, so again no extra lithography is required. The devices were contacted with probe needles for initial characterization. A couple of samples were soldered on submounts, allowing them to be mounted into butterfly packages for system characterization.

Leakage currents were obtained by imposing a direct bias in one of the photodiode and monitoring the other. Up to 10 mA is injected. Without grounding the guard rings, there is about 600–700 µA flowing through PD2 (forced at zero bias) when PD1 is biased for 10 mA, and vice-versa. With the guard rings grounded, there is a gain of 20–40 and cross-currents diminish to the 15–30 µA range. The behaviour is not linear (i.e. the cross-talk depends on current) either with or without guard rings. This is a well-known effect of distributed sheet resistance feeding the distributed diodes equivalent to the underlying junctions, requiring some saturation of the elements near the feed before the farther elements can be reached by current lines and overcome the diode thresholds in spite of the device sheet resistances. These values were therefore not yet satisfying to really operate independently the two photodiodes. With the trenches around PD2, we obtained cross-currents less than 3 µA in the same conditions. This proved much safer to

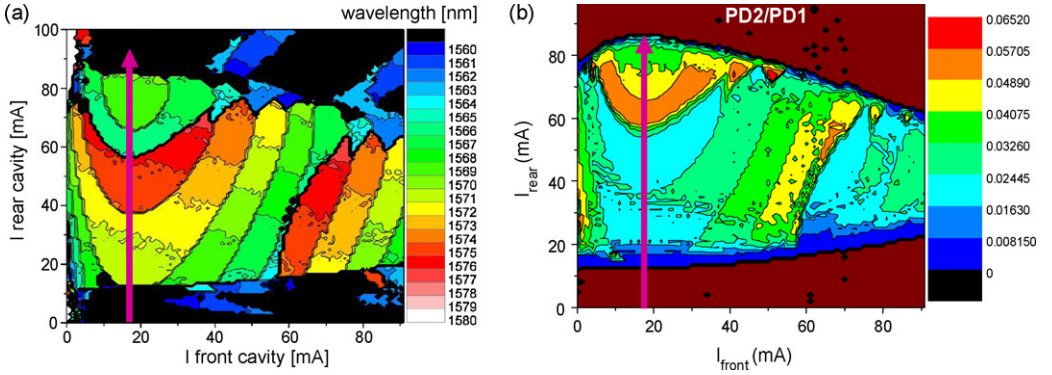

Fig. 6. (a) Wavelength map as a function of current in both sections; (b) map of the photocurrent ratio in the same plane. Note the overall agreement; arrows indicate the scans of Fig. 8.

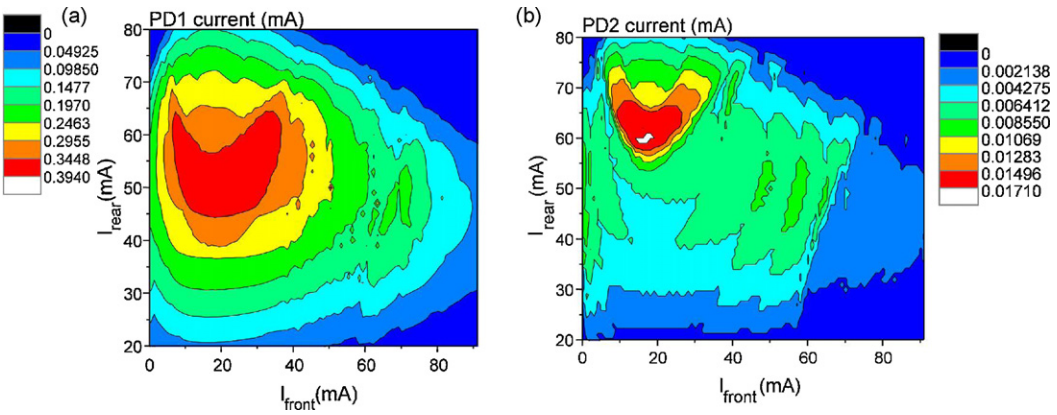

Fig. 7. Maps of the photocurrent of Detector 1 (a) and Detector 2 (b); the lasing wavelength meets the mini-stopband range mainly in the upper left part of the map, hence the localized response.

perform the desired spectral monitoring operations. Hence, it was necessary to implement these trenches for the present integration strategy.

The laser themselves operated as those previously published, with typical output powers in excess of 10 mW over a fair range. This is not the topic of the present paper, though. The wavelength map in the plane of the two-section currents $\lambda = \lambda(I_{\text{front}}, I_{\text{rear}})$ is obtained by means of an automated set-up. It is presented in Fig. 6a. The range covered is 1564–1580 nm. The parabolic shape of the overall plot is a result of the tuning mechanisms as described at the beginning of the paper and in [4].

The next step was to monitor both photodiode currents as a function of laser section currents, with the correlation of photodiode current ratio with wavelength to be extracted only as a final step. The measured maps of photocurrents I_1 and I_2, in photodiodes PD1 and PD2 respectively, are shown in the color maps of Fig. 7a and b, in the same (I_{front}, I_{rear}) plane as the wavelength. The overall pattern of the ''through'' signal in photodiode PD1 reproduces the output power behaviour, centered at (20 and 55 mA). Decrease at higher currents comes from heating effects mainly. There is already a visible scar in the top of this map, caused by the diverted flux into PD2, as we shall see. The scar is rather a power dip and is thus responsible the location of the apparent maximum (red region), which would lie at slightly higher currents without the scar.

The ''drop'' signal of photodiode PD2 (Fig. 7b) has a very distinct map, being noticeable only in the top left region of the (I_{front}, I_{rear}) plane. We therefore have a first signature that the drop is operating preferentially at those wavelengths obtained at the highest power. Hence the device, overall, possesses its best monitoring potential near the maximum power region, which makes sense. The parabolic shape of Fig. 6a is preserved in both maps, although the local variations are much stronger in Fig. 7b. The absolute value of the ''drop'' signal is much weaker than the direct one. This can be partly explained from the optical characteristics of both channel, up to a factor of five ratio or so. We tentatively ascribe the rest of the difference to unwanted recombinations due to etched trenches. This point should be addressed in future designs.

The ratio of the two photocurrents, although weak in absolute terms, is the interesting quantity to monitor, the resulting map being shown in Fig. 6b. It just combines the data of Fig. 7a and b. Visually, the comparison with the wavelength map offers large and striking similarities: the parabolic region at the top is well rendered, as well as the smoother plateau region around (50 and 50 mA). This is a very good indication that our integrated monitor device can properly monitor the laser wavelength.

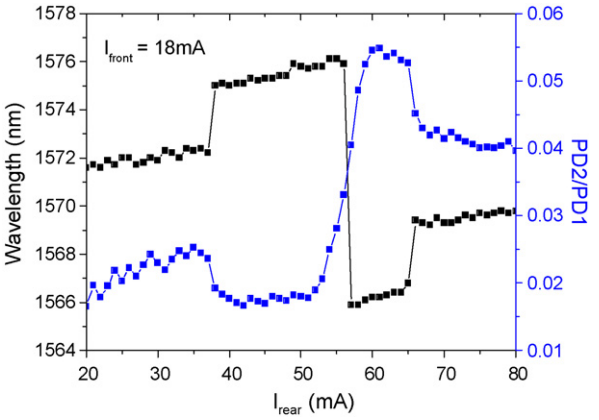

Fig. 8. Scan of rear current at a fixed 18 mA front current (arrow of Fig. 6): wavelength evolution and current ratio evolution.

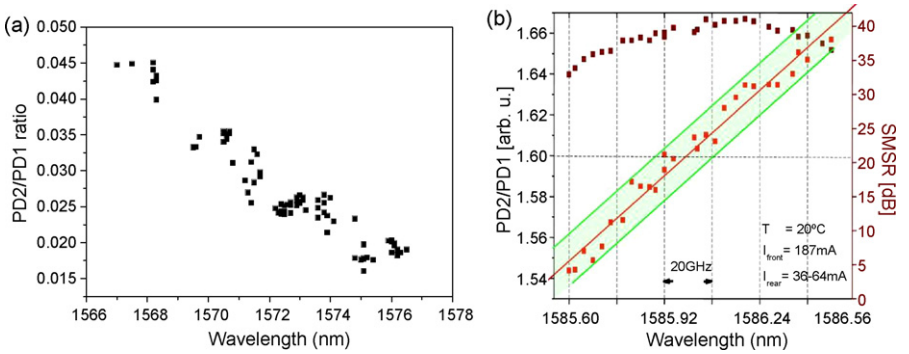

Fig. 9. (a) Overall correlation between wavelength and photocurrent ratio. The fuzzy behaviour around the straight line is partly ascribed to low SMSR situations; (b) correlation plot and SMSR, in a high SMSR ∼1 nm region between mode hops (87 mA front current, 36–64 mA rear current), showing that an upper bound of 20 GHz holds for the fluctuation even using a single basic measurement.

To address this issue in more detail, we have to gather on the same plot the wavelength and the photodiode current ratio I_2/I_1. This ratio is represented in Fig. 8, when scanning along the vertical line (I_{front}= 18 mA, I_{rear}) of Fig. 7. There are four main regions separated by mode hops. Although the wavelength evolution is by far not monotonous, the reader can check on the four plateaus of this data set that the lowest wavelength is associated with the largest ratio, and so on, in correct order.

A more explicit check is the plot of photocurrent ratio against photocurrent ratio, as done in Fig. 9a, when the current is widely varied across several mode hops. Across the 1566–1576 nm scan, the negative relation ship is quite clear. However there are some ambiguities, i.e. the relationship between wavelength and photocurrent ratio is not unequivocal.

There can be several reasons to this behaviour, one of them being the fact that situations with poor SMSR (near mode hops) blur the neater situation between mode hops. We did not make a full test of whether the side mode could perturb the measure by the amount of ‘‘noise’’ visible in Fig. 8, but this assumption seems quite likely. As a support to this conjecture, we plot in Fig. 9b the same ratio vs. wavelength correlation, but on a narrower 1 nm region (125 GHz) of a similar device (larger wavelength by ∼16 nm), displaying also on the same plot the SMSR above 34 dB in the same region. No special precautions were taken to average the photocurrent data, the data used here as just those from the raw global scan. The correlation is quite clear on this device, albeit with the opposite slope as we are essentially on the other side of the MSB. Most points depart by less than 5 GHz of the average trend (red line), and all of them are contained in a 20 GHz wide range. Therefore, stabilization with a similar accuracy (at worse 20 GHz, and even better with some efforts, say less than 10 GHz) seems possible.

At this stage, it appears that the approach chosen does allow proper monitoring information for wavelength stabilization by an external computer, using bookkeeping to reach first a deterministic sub-region in power and wavelength, followed by (slow) feedback from monitor current ratio.

Among the aspects to be further investigated are those related to the feedback loop, and notably its time constant. The photodiodes can be operated in the MHz range without difficulties, so that stabilization down to 1 μs time constant is possible. Ideally, one should grant an absolute wavelength from such monitoring. It is not the case as such because of thermal aspects: the MSB will follow about the same optogeometric drift as the cavity and as typical DFB gratings (0.1 nm/K). However, this can also be compensated by measuring the diode threshold voltage in the dark case, of the order of the energy gap (0.8 eV). It drifts by a few mV/K, so that an ordinary measurement could also exploit it to get the actual chip temperature, and compensate it when using the integrated monitor.

5. Conclusion

We have demonstrated, at telecommunication wavelengths, the feasibility of the monolithic integration on an InP active chip of a tunable laser and a wavelength monitor. Both parts of the chip used the same PhC fabrication step and exploited the same p–n junction designed for laser action. Tunability has been implemented by the Vernier effect between two-gain sections, while two photodiodes were defined with PhC around a wavelength selective design. The selectivity from the MSB-demultiplexing effect in a multimode waveguide

such as W3 was found to be effective for monitoring. The coincidence of the MSB range with the laser tuning range was achieved. The strategy of measuring the two photocurrent and their ratio implied good electrical insulation (guard rings, trenches), whereas the minimization of laser feedback demanded specific arrangements of the entrance of the selective PhC device to frustrate the coherent scattering causing the reflected signal. A good correlation was observed on a 10 nm range, and a 20 GHz overall fluctuation was seen on a 1 nm range when focusing on a large SMSR region. This final data indicate that this kind of monitor is best welcome in arrays of lasers, more and more implemented in today's PICs (photonic integrated circuits). These lasers need a modest tunability, but the frequency comb they address has to fit the ITU grid or any other grid requirement as closely as possible. The real-estate to be added to a standard laser is minute in our approach. We have eventually given some clues to exploit the monitoring action in the presence of temperature drifts: they can in principle be then into account in order to attain the accurate feedback and precise combs desired in such PIC devices.

Acknowledgments

We acknowledge the support of the European project FUNFOX FP6-IST-04582 and the help of O. Khayam in IOGS.

References

[1] L.A. Coldren, G.A. Fish, Y. Akulova, J.S. Barton, L. Johansson, C.W. Coldren, Tunable semiconductor lasers: a tutorial, IEEE J. Lightwave Technol. 22 (2004) 193–202.

[2] M. Kamp, T. Happ, S. Mahnkopf, G.-H. Duan, S. Anand, A. Forchel, Semiconductor photonic crystals for optoelectronics, Physica E 21 (2004) 802–808.

[3] S. Mahnkopf, M. Arlt, M. Kamp, V. Colson, G.H. Duan, A. Forchel, Two-channel tunable laser diode based on photonic crystals, IEEE Photon. Technol. Lett. 16 (2004) 353–355.

[4] S. Mahnkopf, M. Kamp, A. Forchel, F. Lelarge, G.-H. Duan, R. März, Mode anti-crossing and carrier transport effects in tunable photonic crystal coupled-cavity lasers, Optics Commun. 239 (2004) 187–191.

[5] L.A. Coldren, S.W. Corzine, Diode Lasers and Photonic Integrated Circuits, Wiley, New York, 1995.

[6] D.A. Ackerman, K.M. Paget, L.F. Schneemeyer, L.J.-P. Ketelsen, F.W. Warning, O. Sjolund, J.E. Graebner, A. Kanan, V.R. Raju, L.E. Eng, E.D. Schaeffer, P. Van Emmerik, Low-cost a thermal wavelength-locker integrated in a temperature-tuned single-frequency laser package, IEEE J. Lightwave Technol. 22 (2004) 166–171.

[7] H. Ishii, K. Kasaya, H. Oohashi, Y. Shibata, H. Yasaka, K. Okamoto, Widely wavelength-tunable DFB laser array integrated with funnel combiner, IEEE J. Sel. Top. Quantum Electron. 13 (2007) 1089–1094.

[8] A. Talneau, S. Slempkes, A. Ougazzaden, Accuracy on emitted wavelengths in DFB laser arrays resulting from the longitudinal mode selection mechanism, IEEE J. Sel. Top. Quantum Electron. 6 (2000) 191–196.

[9] S. Ménézo, A. Talneau, F. Delorme, S. Grosmaire, F. Gaborit, S. Slempkes, 10-Wavelength 200-GHz channel spacing emitter integrating DBR lasers with a PHASAR on InP for WDM applications, IEEE Photon. Technol. Lett. 11 (1999) 785–787.

[10] C. Schuller, F. Klopf, J.P. Reithmaier, M. Kamp, A. Forchel, Tunable photonic crystals fabricated in III–V semiconductor slab waveguides using infiltrated liquid crystals, Appl. Phys. Lett. 82 (2003) 2767–2769.

[11] M. Kamp, H. Scherer, C. Ulzhöfer, B. Völker, A. Forchel, K. Janiak, H. Heidrich, R. Brénot, G. H. Duan, ''Tunable Photonic Crystal Laser with Integrated Wavelength Monitor,'' presented at ECOC'06, Cannes, 2006.

[12] M. Kamp, H. Scherer, K. Janiak, H. Heidrich, R. Brénot, G.H. Duan, H. Benisty, A. Forchel, Nanophotonic integrated lasers, in: Presented at photonics west, integrated optics: devices, materials, and technologies X, 64750Z, San Jose, February 14, 2007.

[13] E. Viasnoff-Schwoob, C. Weisbuch, H. Benisty, C. Cuisin, E. Derouin, O. Drisse, G.-H. Duan, L. Legouézigou, O. Legouézigou, F. Pommereau, S. Golka, H. Heidrich, H.J. Hensel, K. Janiak, Compact wavelength monitoring by lateral outcoupling in wedged photonic crystal multimode waveguides, Appl. Phys. Lett. 86 (2005) 101107.

[14] S. Olivier, M. Rattier, H. Benisty, C.J.M. Smith, R.M. De La Rue, T.F. Krauss, U. Oesterle, R. Houdré, C. Weisbuch, Mini stopbands of a one-dimensional system: the channel waveguide in a two-dimensional photonic crystal, Phys. Rev. B 63 (2001) 113311.

[15] L. Martinelli, H. Benisty, O. Khayam, G.H. Duan, H. Heidrich, K. Janiak, Analysis and optimization of compact demultiplexer monitor based on photonic crystal waveguide, IEEE J. Lightwave Technol. 25 (2007) 2385–2394.

[16] M. Ayre, C. Cambournac, O. Khayam, H. Benisty, T. Stomeo, T.F. Krauss, ''Photonic crystal waveguides for coarse-selectivity devices,'', Photon. Nanostruct. Fundam. Appl. 6 (2008) 19–25.

[17] H. Benisty, A. David, L. Martinelli, E. Viasnoff-Schwoob, C. Weisbuch, G.-H. Duan, K. Janiak, H. Heidrich, From modal control to spontaneous emission and gain in photonic crystal waveguides, Photon. Nanostruct. Fundam. Appl. 4 (2006) 1–11.

[18] T. Stomeo, F.V. Laere, M. Ayre, C. Cambournac, H. Benisty, D.V. Thourhout, R. Baets, T.F. Krauss, Integration of grating couplers with a compact photonic demultiplexer on an InP membrane, Opt. Lett. 33 (2008) 151–156.

[19] T.D. Happ, M. Kamp, A. Forchel, Photonic crystal tapers for ultracompact mode conversion, Opt. Lett. 26 (2001) 1102–1104.

[20] http://www.photondesign.com/products/crystalwave.htm.

[21] X. Checoury, A. Chelnokov, J.M. Lourtioz, Fine structural adjustment of lasing wavelengths in photonic crystal waveguide laser arrays, Photon. Nanostruct., Fundam. Appl. 1 (2003) 63–68.

[22] S. Olivier, H. Benisty, C. Weisbuch, C.J. Smith, T.F. Krauss, R. Houdré, Coupled-mode theory and propagation losses in photonic crystal waveguides, Opt. Exp. 11 (2003) 1490–1496.